Range of “complete” instability of flat flames propagating downward in the acoustic field in combustion tube: Lewis number effect

Ajit Kumar Dubey[1], Yoichiro Koyama[1], Sung Hwan Yoon[2], Nozomu Hashimoto[1], Osamu Fujita[1]

[1]Division of Mechanical and Space Engineering, Hokkaido University

Kita 13 Nishi 8, Kita-ku, Sapporo, Hokkaido, 060-8628, Japan

[2]Division of Marine System Engineering, Korea Maritime and Ocean University

727 Taejong-ro, Dongsam 2(i)-dong, Yeongdo-gu, Busan, 49112, Republic of Korea

Corresponding author: Osamu Fujita

Division of Mechanical and Space Engineering, Hokkaido University, Kita 13 Nishi 8 Kita-ku, Sapporo, Hokkaido, 930-8555, Japan

TEL: +81-11-706-6385

FAX: +81-11-706-7841

E-mail: ofujita@eng.hokudai.ac.jp

Abstract

Downward propagating flames ignited at the open end of an open-closed tube exhibit thermo-acoustic instability due to interaction of combustion generated acoustic fluctuations with the flame front. At sufficiently high laminar burning velocity (S_L) two regimes of thermo-acoustic instability are observed, namely, primary instability (where initial cellular flame transitions to a vibrating flat flame) and a secondary instability (where vibrating flat flame transitions to vibrating turbulent flame due to parametric instability of flame front). On further increasing S_L to a particular value, "complete instability" of flat flames is observed meaning flat flame cannot be stabilized and initial cellular flame transitions directly to parametric instability. This particular S_L introduced in this work is termed "critical S_L". In past experimental works, stability of flat flames in the acoustic field had only been studied in terms of acoustic velocity amplitude and a critical acoustic velocity amplitude had been measured at the onset of parametric instability. The novelty of this work is that boundary of unconditional instability of flat flame (flat flame is unstable irrespective of acoustic velocity amplitude) is determined in terms of mixture conditions e.g. S_L. Particularly for propagating flames, this critical S_L can be measured more easily and accurately than the critical acoustic velocity. This work presents the effect of *Le* (Lewis number) on critical S_L. Three different fuels, CH_4, C_2H_4 and C_3H_8 are tested with two different dilution gases (N_2 and CO_2) for equivalence ratio of 0.8 (lean) and 1.2 (rich). Twelve different *Le* ranging from 0.7 to 1.9 are generated through these mixture combinations. Generally, larger *Le* mixtures show higher critical S_L than lower *Le* mixtures for any fuel. Theoretical calculations are performed to predict critical S_L by studying instability of planar flame fronts in presence of acoustic forcing. Theoretical calculations successfully captured the effect of *Le* as predicted stability region of planar flame is narrower for lower *Le* than that for higher *Le*. However, accurate quantitative predictions of critical S_L couldn't be obtained from existing theory, particularly for non-unity *Le*. Hence, a correction (a function of Zeldovich number, β and *Le*) to width of stability region is proposed to obtain better quantitative agreement for critical S_L between experiments and theory and performs significantly well. The correction factor acts to compensate for the inaccuracies in Markstein number obtained from an analytical relationship during calculation of stability region width.

Keywords: Premixed combustion, Thermo-acoustic instability, Parametric instability, Laminar burning velocity, Markstein number

1. Introduction

Thermo-acoustic instability occurs due to coupling of combustor acoustics with unsteady combustion [1] [2] and can be a major challenge for design and operation of various practical combustors. The occurrence of thermo-acoustic instability is governed by Rayleigh criterion [3] which states that if the integral of product of fluctuating pressure and heat release are positive over a cycle, amplitude of acoustic fluctuations would be amplified. The flame-acoustic coupling can be studied in a simple experiment where a flame ignited at open end propagates downward towards the closed end of the tube. This system is prone to thermo-acoustic instability as was demonstrated by Searby [4]. The simplicity of this experiment is due to possibility of quiescent combustible mixture which leads to a laminar flow field ahead of flame front and the fluid flow is only due to self-generated acoustics. Instabilities due to inlet turbulence and vorticity production at burner inlet as well as equivalence ratio fluctuations do not exist because it is not a continuous flow experiment. This simplicity renders it amenable to theoretical analysis of flame instability considering the laminar flame structure in detail through large activation energy asymptotic [5]. Two kinds of thermo-acoustic instabilities are observed during downward propagation of flames ignited at open end in tubes, namely, primary acoustic instability and secondary acoustic instability [4]. Primary instability is observed for moderate laminar burning velocity (S_L) mixtures and primary instability is followed by secondary instability for sufficiently higher S_L mixtures. During primary acoustic instability, the hydrodynamic (D-L) instability of flame front is suppressed by self-generated acoustic fluctuations and flame oscillates with acoustic frequency. This primary instability can transition to secondary instability if acoustic fluctuations are sufficiently higher. The secondary acoustic instability is caused by parametric instability of flame front where structures on the flame front oscillate at half the acoustic frequency and lead to formation of turbulent fluctuating flame. Growth rates of acoustic fluctuations and peak pressure amplitudes are considerably higher during secondary acoustic instability compared to primary acoustic instability.

Since, the experimental work of Searby [4] several studies have been performed to generate better understanding of the thermo-acoustic phenomena in downward propagating flames. Pressure coupling [6-8] and velocity coupling [9] were studied as possible mechanisms for primary acoustic instability. Nonlinear coupled equations were later derived considering both these mechanisms [10] and later studied for weakly non-linear case [11]. Some aspects of experimental observation e.g. appearance of secondary instability after primary instability were predicted. Effect of tube length and diameter on thermo-acoustic instability was also studied [12]. Parametric instability of higher acoustic modes was also observed for gaseous [13] and spray flames [14]. Growth rates of primary acoustic instability [14] and secondary acoustic instability [13] had also been reported and compared with theoretical prediction based on velocity coupling mechanism [9]. It is now positively established that acoustic instability in propagating flames is mostly due to change in flame front surface due to interaction with acoustic field. Thermoacoustic instabilities were also reported for downward propagating flames in the annulus between two cylinders for quiescent [15] [16] and turbulent mixture conditions [17]. H_2/air mixtures in vertical square channel showing thermoacoustic instabilities had also been studied [18]. Recently, oscillatory flame propagation has also been reported in very narrow channels called Hele-Shaw cells [19]. Application of laser irradiation to propagating flame can artificially modify the flame surface and cause transition to turbulent flames through parametric instability [20] [21] [22]. The laser irradiation method has also been used to study the onset of primary instability [23], Lewis number effect on primary instability [24][25] and transition from primary to secondary instability [26].

In our earlier works [12,13, 23, 24], we mainly discussed the thermoacoustic instability i.e. growth of pressure fluctuations during downward propagation of flames. In these experiments, flame front also shows instabilities due to interaction with acoustic field. In the present work, we are concerned with flame-front instabilities in presence of acoustics. Theoretical framework for studying effect of acoustic (periodic) acceleration on stability of planar flame front was first established by Markstein [27]. The equations can

be reduced to Mathieu's equation. Two regimes of planar flame front instability, hydrodynamic and parametric were clearly predicted. Searby and Rochwerger [28] extended the theory in light of thin-flame model and provided analytical relations for the parameters in the Mathieu's equation for parametric instability. They also studied parametric instability experimentally in a stabilized flame setup for lean propane/air mixtures [28]. The wavenumber of flame cells and acoustic velocity amplitude at the onset of parametric instability were well predicted. Computation of these stability limits requires a numerical solution [28]. Nonetheless, analytical solution was developed for acoustic parametric instability of flame front in the limit of high frequency acoustic oscillations [29]. Regime diagrams were also presented for methane/air mixtures using the analytical solution [16]. However, the acoustic velocity measured using LDV in propagating flame experiments a) at onset of parametric instability and b) at disappearance of hydrodynamic instability did not compare qualitatively or quantitatively with analytical predictions. A major reason for such discrepancy was believed to be incorrect prediction of Markstein number using Clavin-Williams theory [5] (Eqn. 7 in this work). The acoustic velocity measurements at onset of parametric instability was also used to predict Markstein number of methane/air mixtures [30]. Parametric instability of flame front in H_2/air mixtures [31] were also studied using Searby & Rochwerger model [28] but any quantitative comparison with experiments was not reported. Hence, further work is required to test and attain quantitative agreements between theory and experiments on stability of flat flames in acoustic field for various mixture conditions and acoustic field. Earlier works have only used acoustic velocity and wavenumbers of flame structure at the onset of parametric instability [16] [28] to compare theory and experiments. In this work, we introduce a new parameter which can be used to test the theory, namely, S_L at onset of "complete instability". Complete instability is said to occur when flat flame cannot be stabilized anywhere in the tube during propagation and transition to parametric instability happens directly from initial cellular flame. Theoretically, during complete instability, there exists a range of wavenumber which is either hydrodynamically or parametrically unstable irrespective of acoustic velocity

fluctuation amplitude. Such complete instability is observed at burning velocity of 42 cm/s in Searby's work [4] and in regime V or above from our earlier work [12] [13] where flat flame could not be observed during flame propagation. S_L at onset of "complete instability" can be influenced by Lewis number which provides a way to study effect of Lewis number on acoustic parametric instability.

Hence, this work presents an experimental and theoretical study on effect of Lewis number, *Le* on transition to "complete instability" in downward propagating flames in tubes. Stability diagrams and predictability of critical S_L for different *Le* mixtures are discussed. An important aspect of present work is that "critical S_L" introduced in present work is fairly easy to measure compared to acoustic velocity at onset of parametric instability, particularly for propagating flames. We assess effect of *Le* which is an easily calculable parameter, whereas in earlier works [16, 28] Markstein number was used as a parameter which had to be estimated using different experiments or simulations.

2. Experimental method

Experimental setup is schematically shown in Fig. 1. The experimental setup is similar to our earlier works [12] [13]. It consists of a transparent acrylic vertical combustion tube of length 711 mm and diameter 50 mm. The combustion tube was closed at bottom and a lid was fixed on springs on the upper side which can be opened by the action of an electromagnet. The tube was filled with test mixture through metered gas flows for all constituents and around five minutes was allowed for the mixture to become quiescent. Then, the test mixture was ignited at the top end by an electric spark and simultaneously, the top lid was opened. So, the tube had open-closed boundary condition during flame propagation from top to bottom end. The downward propagating flame was recorded by a high-speed camera (FASTCAM Mini UX100) at 2000 frames per second. Pressure fluctuations were also measured with a PCB Piezotronics 106B52 dynamic pressure sensor located at the bottom end of the tube at a sampling rate of 10 kHz.

Three fuels CH_4, C_2H_4 and C_3H_8 were used with O_2 as the oxidizer at equivalence ratio of 0.8 and 1.2. The equivalence ratio is defined as $\Phi = \frac{(Fuel/O_2)}{(Fuel/O_2)_{st}}$ N_2 and CO_2 were used separately as diluents and their dilution was varied to obtain different laminar burning velocity (S_L) of the fuel/air mixtures at constant equivalence ratios of 0.8 and 1.2. Twelve different Lewis number, *Le* were obtained by varying fuel, equivalence ratio and diluent gas ranging from 0.76 to 1.86. S_L was calculated for all the mixture conditions with chemical kinetic mechanism of USC II [32] using CHEMKIN Pro. All the mixture compositions and their properties are tabulated in Appendix. Experimental results for all CH_4 mixtures, $C_3H_8/O_2/CO_2$ mixtures and rich $C_2H_4/O_2/N_2$ mixtures are presented for the first time. Experimental observations with $C_3H_8/O_2/N_2$ mixtures [25], lean $C_2H_4/O_2/N_2$ mixtures [24], lean $C_2H_4/O_2/CO_2$ mixtures [12,13,24] and rich $C_2H_4/O_2/CO_2$ mixtures [13, 24] have also been presented in our earlier works.

3. Analytical method

A planar or flat flame is only observed under certain mixture conditions and at certain flame locations during experiments of downward propagating flames in a tube. The instability (deviation from planar flame) can arise due to internal cause (hydrodynamic and thermo-diffusive instability) or external cause (due to action of self-generated acoustic fluctuation on the flame front). Lot can be learnt about flame propagating in self-generated acoustic field by formulating and solving the stability problem of a planar flame front which is subjected to acoustic velocity perturbations. Time evolution equation of premixed flame front whose location is represented by (α) subjected to periodic acoustic forcing was derived by Searby and Rochwerger [28] based on flame model of Searby and Clavin [33] and is written as

$$A\frac{\mathrm{d}^2\alpha}{\mathrm{d}\,t^2} + B\frac{\mathrm{d}\alpha}{\mathrm{d}t} + \{C_0 - C_1\, cos(\omega_a t)\}\alpha = 0 \tag{1}$$

Where analytical functions are defined as [28]

$$A = (2-\gamma) + \gamma \boldsymbol{k}(Ma - \frac{J}{\gamma}) \tag{2}$$

$$B = 2\boldsymbol{k} + 2\frac{\boldsymbol{k}^2}{1-\gamma}(Ma - J) \tag{3}$$

$$C_0 = \frac{\gamma \boldsymbol{k}}{Fr}\left[1 - \boldsymbol{k}\left(Ma - \frac{J}{\gamma}\right)\right] - \frac{\gamma}{1-\gamma}[\boldsymbol{k}^2 - \boldsymbol{k}^3\{h_2 + \frac{\gamma+2}{\gamma}Ma - \frac{2J}{\gamma} + (2Pr-1)\int_0^1 \big(h_2 - h(\theta)\big)\mathrm{d}\theta\}\,] \tag{4}$$

$$C_1 = \gamma \boldsymbol{k}\omega_a U_a[1 - \boldsymbol{k}\left(Ma - \frac{J}{\gamma}\right)] \tag{5}$$

Here, $\gamma = \frac{\rho_1 - \rho_2}{\rho_1}$, $\rho_{1,2}$ is density. The subscripts 1 and 2 refer to unburnt and burnt sections of the gas. $\boldsymbol{k}$ is wavenumber normalized by flame thickness, $d = \frac{D}{S_L}$, $D$is thermal diffusivity of unburnt mixture calculated

using mixture-average formulation. Fr is Froude number defined as $\frac{S_L^2}{gd}$, g is gravitational acceleration taken as 980 cm/s^2. Pr is Prandtl number. ω_a is the acoustic circular frequency obtained from experiments normalized by flame transit time, $\frac{d}{S_L}$. U_a is the imposed acoustic fluctuation velocity amplitude normalized by S_L. Also, $\theta = \frac{T-T_1}{T_2-T_1}$, is the normalized temperature, $h(\theta) = \frac{(\rho D)_\theta}{(\rho D)_{\theta=0}}$, h_2 is $h(\theta)$ in burnt gas. $h(\theta)$ for all the employed mixtures were calculated using CHEMKIN libraries as a function of θ. Once $h(\theta)$ is known for a mixture, following integrals can be computed [28]

$$J = \frac{\gamma}{1-\gamma}\int_0^1 \frac{h(\theta)}{1+\theta\frac{\gamma}{1-\gamma}}\mathrm{d}\theta \tag{6}$$

Also, Ma, the non-dimensional Markstein number is defined as [28]

$$Ma = \frac{J}{\gamma} - \frac{1}{2}\beta(Le-1)\int_0^1 \frac{h(\theta)ln(\theta)}{1+\theta\frac{\gamma}{1-\gamma}}\mathrm{d}\theta \tag{7}$$

Here, β is Zeldovich number defined as $\beta = \frac{E(T_2-T_1)}{R(T_2)^2}$, non-dimensional activation energy, $\frac{E}{R} = 2(T_2)^2\frac{d[ln(\rho_1 S_L)]}{d[T_2]}$, which is calculated by calculating S_L using USC II mechanism for various initial temperatures T_1which changes T_2 and then calculating the relevant gradient. Le is Lewis number, defined as $Le = \frac{D}{D_m}$, D_m being mass diffusivity of deficient reactant in dilution gas (N_2 or CO_2) at unburnt mixture conditions. It might be argued to consider an effective *Le* as in [19],however, the critical S_L with both effective *Le* and *Le* based on deficient reactant were same. So, we have used the *Le* based on deficient reactant. . Values of β and Le are tabulated in Appendix A for each mixture employed in this work.

Markstein length in dimensional form can be found by multiplication of Ma and d. Ma for selected mixtures is also tabulated in Appendix.

On making the following substitution [28]

$$\mathrm{z} = \frac{1}{2}\omega_a \mathrm{t} \qquad \varphi = \frac{B}{A\omega_a} \qquad a = \frac{4AC_0 - B^2}{(A\omega_a)^2} \qquad q = \frac{2C_1}{A\omega_a^2} \tag{8}$$

$$\alpha = \mathrm{Y(z)e^{-\varphi z}e^{iky}}$$

Equation 1 is transformed to well-known Mathieu's equation representing a parametric oscillator [27] [28]

$$\frac{\mathrm{d}^2\mathrm{Y}}{\mathrm{d\,t}^2} + \{a - 2q\,cos(2\mathrm{z})\}\mathrm{Y} = 0 \tag{9}$$

The method of finding stability is based on [31]. A solution of following form is assumed

$$Y(z) = e^{i\mu z} \sum_{\mathrm{k}=-\infty}^{+\infty} P_{2k} e^{i2\mathrm{kz}} \tag{10}$$

For $Y(z)$ to be a solution of Mathieu's equation the variable μ should satisfy the following equation [34]

$$\cos(\pi\mu) = 1 - \Delta(0, a, q)(1 - \cos(\pi\sqrt{a})) \tag{11}$$

Here, for an arbitrary r, $\Delta(\mu, a, q, r)$ is given by following tridiagonal matrix

$$\begin{vmatrix}
1 & l_{2r} & \cdots & & & & & & \\
l_{2(r-1)} & 1 & l_{2(r-1)} & \cdots & & & & & \\
\vdots & \vdots & \ddots & & & & & & \\
 & & l_{-2} & 1 & l_{-2} & & & & \\
 & & & l_0 & 1 & l_0 & & & \\
 & & & & l_2 & 1 & l_2 & & \\
 & & & & & & \ddots & & \\
 & & & & & & l_{2(r-1)} & 1 & l_{2(r-1)} \\
 & & & & & & & l_{2r} & 1
\end{vmatrix} \tag{12}$$

with $l_{2r} = \frac{q}{(2r-i\mu)^2-a}$. $\Delta(0,a,q)$ can be found by setting $\mu = 0$ in above matrix. And in this case l_{2r} becomes an even function i.e. $l_2 = l_{-2}$ and so on. This matrix is an infinite matrix as r is ∞. Fortunately, the matrix can be calculated by a three-point recursive formula suggested by Strang [35].

$$\Delta(0,a,q,r) = n_{2r}\Delta(0,a,q,r-1) - m_{2r}n_{2r}\Delta(0,a,q,r-2) + m_{2r}m_{2(r-1)}^2\Delta(0,a,q,r-3) \quad (13)$$

Here, $m_{2r} = l_{2r}l_{2(r-1)}$, and $n_{2r} = 1 - m_{2r}$. The value of r should be large enough to find a good estimate of $\Delta(0,a,q)$. In practice, a converged value is obtained for small value of r. In this work we use $r = 20$. Once, $\Delta(0,a,q)$ is obtained, stability factor, F, can be calculated

$$F = \frac{1}{\pi}\text{acosh}\left(1 - \Delta(0,a,q)\left(1 - \cos\left(\pi\sqrt{a}\right)\right)\right) - \frac{B}{A\omega_a} \quad (14)$$

The condition for marginal stability is given by $\mu = \varphi$ i.e. $F = 0$. For a given wavenumber $\boldsymbol{k}$ and acoustic forcing U_a, it can be determined whether the system is stable or unstable based on whether F is negative or positive. The stability boundary can be obtained in $\boldsymbol{k} - U_a$ plane. Such results are shown in section 4.2 along with contours of F.

4. Results and discussion

4.1 Experimental flame regimes and "critical S_L"

It is well known that flames ignited at open end of a tube and propagating towards closed end are prone to thermo-acoustic instability. The combustion generates acoustic disturbances which interact with the propagating flame front to give various interesting shapes of flame front. Six different flame propagation

regimes are observed in current experiments by changing S_L of test mixture for various fuel and dilution conditions. These are named sequentially from Regime I to VI.

Figure 2 shows a few representative flame images at different times of propagation during unstable flame propagation regimes i.e. regime II to regime VI. Flame images at some selected time are cropped and placed below one another to give an idea of how the flame changes during propagation. The frames are selected to represent the various flame shape changes during a particular regime. The videos of propagating flames for Regime I to VI are provided as supplementary files for complete observation. Figure 3 shows pressure fluctuations associated with regimes I to regime VI. Flame dynamics during these regimes have also been explained in our previous works [12] [13]. Nevertheless, a brief description is required for self-sufficiency and clear understanding of this work.

During regime I (Fig. 3(a)), a curved flame propagates from open to closed end and no acoustics is generated. Flame images at various instances of propagation are similar to that in regime II shown in Fig. 2(a), so they are not shown here. During regime II (Figs. 2 (a), 3(b)), curved flame starts vibrating after some time from ignition due to interaction with self-generated acoustics. Both pressure oscillation and flame oscillation correspond to fundamental mode of tube. During regime III (Figs. 2(b) 3(c)), curved flame after ignition transitions to a vibrating flat flame which propagates until the end of tube; the pressure oscillation amplitude increases during this transition and then saturates. This is called the primary acoustic instability during which the amplitude of initial curved flame decreases leading to a vibrating flat flame. During regime IV (Figs. 2 (c) 3(d)), curved flame after ignition transitions to a vibrating flat flame; when this flat flame reaches around center of tube, corrugated structures develop on the flame front and flame quickly transitions to a turbulent vibrating flame. This transition generates high amplitude pressure oscillations called secondary instability. During secondary instability, the structures on the flame front oscillate with half the acoustic frequency due to parametric instability of flame front, similar to Faraday instability. Typical pressure fluctuations associated with regimes II to IV are similar to that reported by

Searby [4] and Yáñez [18]. During regime V (Figs. 2 (d) 3(e)), the initial curved flame starts vibrating very soon after ignition, and corrugated structures develop on the curved flame fronts leading to secondary instability. Importantly, flat flame is not observed during regime V indicating that the stability of flat flames is lost. Onset of this regime is later used to define a critical S_L. Regime VI (Figs. 2 (e) 3(f)) is an example of higher harmonic oscillations in the tube where a secondary instability of first harmonic is followed by secondary instability of fundamental mode. More details on higher mode instability can be read from our previous work [13]. The maximum pressure amplitude increases with increase in regime number from I to VI. Figure 4 shows spectral characteristics of pressure fluctuations for regime IV of rich $C_3H_8/N_2/O_2$ mixture. The pressure fluctuations correspond to fundamental mode of the tube of length 711 mm. The frequency increases ranging from 150 to 230 Hz for regime II to V with increase in S_L and regime number due to increase in overall temperature of gases.

Figure 5 summarizes the flame regimes observed in experiments for all mixture conditions showing effect of *Le*. The instability increases as S_L is increased sequentially from a lower value, except for high *Le* mixtures, where regime III is observed for some S_L values higher than the S_L where regime IV is observed. Lower *Le* mixtures transition to primary acoustic instability (onset of regime II/III) at lower S_L. In the present work, we are concerned with transition to regime V, where stability of flat flames is lost. For any *Le* condition, as the S_L is increased at a constant equivalence ratio from a lower value, transition from regime III or IV to regime V is observed at some particular S_L. This S_L is called "critical S_L" and is shown in Fig. 5 by dashed lines for all *Le* cases. Critical S_L can be formally defined as the S_L of mixture above which flat flame cannot be stabilized i.e. lowest S_L for which regime V can be observed. Here, critical S_L can also be seen as a critical mixture condition or CO_2/N_2 dilution ratio at a constant equivalence ratio. In the earlier experimental works, stability of flat flame in acoustic field was characterized only in terms of acoustic fluctuation amplitude [16, 28]. The unique and novel point about present work is that unconditional instability of flat flames in acoustic field is experimentally determined in terms of mixture

conditions (S_L). Here unconditional instability means that flat flame is unstable irrespective of acoustic fluctuation amplitude. It is essential to understand that "critical S_L" is not the S_L where transition to secondary instability is first observed (regime IV in current work), rather the S_L where transition to secondary instability without the occurrence of planar/flat flame is first observed.

The experimental determination of critical S_L is done by observing the flame propagation as S_L is increased for each *Le* mixture and noting the onset of regime V i.e. minimum S_L where transition to parametric instability happens without occurrence of flat flame. Since, the flame images are captured at 2000 frames per second (much higher than acoustic frequency), the S_L where flat flame is not observed during transition to parametric instability can be easily and accurately determined. Occurrence of regime V is also confirmed by pressure measurements. During regime V, pressure increases continuously after ignition and a clear difference between pressure fluctuations between regime V and other regimes is found, as can be seen from Fig. 3. Experiments were repeated at least three times for around half of mixtures and critical S_L measurements were found reproducible. S_L is changed in steps of 2.5 cm/s during experiments, so, maximum error in determination of critical S_L would be ±1.25 cm/s if we assume critical S_L to be midway between two values of S_L where regime change to regime V is observed.

Under similar mixture conditions, higher *Le* mixtures show higher critical S_L i.e. rich CH_4 flames and lean C_3H_8 and C_2H_4 flames have higher critical S_L than lean methane and rich propane and ethylene flames respectively. Critical S_L is an important quantity, as, above critical S_L, the growth rate of instability increases very quickly due to occurrence of secondary instability and there is no mechanism to stabilize this growth. The growth rate of secondary instability and the corresponding maximum pressure is much higher than that during primary instability. Hence, its prediction can be of practical importance and is the objective of this work.

Figure 6 highlights the effect of dilution gas on critical S_L. N_2 diluted mixtures have higher critical S_L than CO_2 diluted mixtures with similar *Le*, hence, they are more stable with respect to thermo-acoustic instability at same S_L. This first appears counterintuitive because CO_2 addition, usually leads to reduced S_L [36] and flame temperature, thus, increased stability [37]. However, in the present work, we treat S_L as an independent parameter in both N_2 and CO_2 dilution experiments. So, the volume fraction of CO_2 in CO_2 diluted mixtures is much less than volume fraction of N_2 in N_2 diluted mixtures for similar S_L. This can be confirmed from tabulated data in Appendix for all fuels. Hence, due to lower dilution, the CO_2 diluted mixtures have higher adiabatic flame temperatures than N_2 diluted mixtures for same S_L (see Appendix) leading to higher coupling constant and, thus, higher instability for CO_2 diluted mixtures [24].

Generally, fuel/air (O_2+3.76 N_2) mixtures are employed in experiments to study thermo-acoustic instability in propagating flames by changing the equivalence ratio [4][16][19]. So, it is useful to look at how critical S_L (or critical equivalence ratio) could be characterized in such experiments. In such experiments, S_L changes with equivalence ratio and it is possible that the critical S_L could be achieved twice over range of flammable equivalence ratios, one each in lean and rich mixture due to different *Le* in lean and rich mixtures. So, complete instability will be observed above (below) critical equivalence ratio in lean (rich) mixtures. Let's consider experiments with propane/air mixtures by Searby [4], where transition to parametric instability from initial curved flame was reported for equivalence ratio of 1.0 (S_L=42.0 cm/s). For equivalence ratio of 0.77 (S_L=27.5 cm/s), regime IV was found in [4]. So, in their experiments, critical S_L should lie somewhere between 27.5 and 42.0 cm/s or equivalence ratio of 0.77 and 1.0. (Consistent with [4], we found critical S_L for lean $C_3H_8/O_2/N_2$ mixtures to be 38.75 ±1.25 cm/s.) If this experiment was continued with increasing equivalence ratio, another critical S_L could be found. But, the critical S_L in rich conditions will be lower than critical S_L in lean conditions. Because, the *Le* of the deficient reactant in lean propane/air mixtures is around 1.8 and that in rich mixtures is around 1.0. And,

for lower *Le*, the critical S_L is also lower based on our experiments. However, it is also possible that critical S_L is observed only once or not at all depending on maximum S_L of the fuel/air mixture. For example, consider CH_4/air flames with maximum S_L of around 37 cm/s near stoichiometry and S_L decreases with increase in equivalence ratio. So, in rich CH_4/air mixtures, S_L will always be lower than critical S_L ~ 37 cm/s measured in current experiments for rich $CH_4/O_2/N_2$ mixtures of equivalence ratio 1.2 and complete instability will not be observed in rich conditions. Transition to secondary instability was also not observed for rich CH_4/air mixtures by recent experiments in Hele-Shaw cell [19] indicating lesser propensity of rich mixtures to transition to secondary instability. Moreover, for fuels with very low burning velocity like ammonia it may not be possible to observe critical S_L with fuel/air mixtures. Obviously, in our experiments it is possible to get critical S_L at many equivalence ratios because we control the S_L by controlling the amount of dilution by N_2 or CO_2. So, at any equivalence ratio we can systematically change the dilution to get a critical S_L.

Geometry and scale of propagating flame experimental setup will also affect the critical S_L. For example, regime V was not observed in annular combustor of gap 1.1 cm for CH_4/air flames over range of equivalence ratios, but regime IV was observed [16]. However, we observed regime V for CH_4 /O_2/N_2 flames in both rich and lean conditions for inner diameter of 5.0 cm. In small annular gap, the wall from both sides lead to higher acoustic losses and instability was suppressed. For circular tubes, the losses increase significantly if tube diameter decreases below 3 cm. Pertaining to the length of tube, Searby and Rochwerger [28] found that fundamental mode of 50 cm tube had higher acoustic losses. In our previous work [12], it was also found that instability reduces significantly for tube lengths below 50 cm. Hence, the length of tube should be more than 50 cm to give critical S_L independent of length of tube. Similarly, instability similar to regime V was not reported in Hele-Shaw cell experiments of gap thickness ≤1.0 cm, but regime IV was reported. Also, the peak pressure amplitudes are almost two to three times lower in Hele-Shaw cell experiments for similar S_L of C_3H_8/air mixture which signifies the effect acoustic losses

due to smaller gap widths and larger open-end area leading to higher wall and radiation losses compared to present experiments. Thus, critical S_L would be higher in small-scale experiments. It is important to measure critical S_L independent of geometry and scale to compare with theoretical analysis which assumes infinite quasi-planar flame without the effect of heat and acoustic loss. Moreover, direction of gravity can also have some effect on flame instability and thus critical S_L but is out of scope of this work.

4.2 Stability regimes: effect of *Le*

Searby & Rochwerger [28] had already established that the parametric instability is the mechanism of stabilization of flat flame during propagating flame experiments under present boundary condition. The acoustic velocity [28,30] and the wavenumbers of corrugated structures [30] at the onset of parametric instability had been successfully predicted by the analytical method presented in last section. Comparison between measured wavenumbers and predicted wavenumbers using analytical method discussed in section 3 is also shown in Fig. 7 for selected mixtures to ensure the equivalence between experiments and theory. The SL chosen are just below critical SL. The measured wavenumbers are in good agreement with the analytical predictions. It indicates that the theory works well for current experimental conditions.

Then, stability regime diagrams for the present mixtures are computed using the method presented in section 3 to understand and predict the influence of *Le* on complete instability.

Figure 8 shows stability diagrams for three characteristic *Le* mixtures of 1.86, 1.03 and 0.76 at a constant S_L of 20 cm/s. The range of unstable wavenumbers for a particular value of acoustic forcing can be observed. As the instability grows with increasing S_L and regime number, acoustic pressure amplitude and forcing acoustic velocity also increase. D-L instability at lower wavenumbers is predicted for low acoustic forcing for all *Le,* and larger wavenumbers are stabilized by the diffusion process. This corresponds to the experimental observation of cellular or non-planar flame close to open end of tube in all regimes (see Fig. 2). *Le* effect is clearly observed in the calculations, as the range of wavenumbers susceptible to

hydrodynamic instability increases with decreasing *Le* of mixtures owing to thermo-diffusive instability. The range of wavenumbers for hydrodynamic instability decreases with increasing acoustic forcing i.e. acoustic forcing stabilizes the hydrodynamic instability. This hydrodynamic instability vanishes at a certain acoustic forcing leading to formation of vibrating flat flames. The acoustic forcing at which hydrodynamic instability is completely eliminated only changes slightly with change in *Le*. Flat flame can be obtained if there exists a range of acoustic forcing for which all the wavenumbers are stable, as in the first two instability diagrams for *Le* >1 and *Le*~1 respectively in Fig. 8. This corresponds to the observation of flat flame in experiments in regime III and IV and shown in Fig. 2 (b) (c). As *Le* decreases, the range of acoustic forcing for which flat flame can be observed reduces significantly and vanishes for *Le* <1 in Fig. 8 for S_L=20.0 cm/s. If acoustic forcing is further increased, onset of parametric instability is observed at a specific wavenumber. The minimum acoustic forcing to cause parametric instability is found to be a strong function of *Le* and decreases significantly with decreasing *Le*. Hence, the onset of parametric instability is expected to happen sooner or closer to open end of tube for lower *Le*. Similar observations are made in experiments.

4.3 Critical S_L: Comparison between theory and experiments

For theoretically predicting the critical S_L, the regime diagram is computed for various S_L and *Le* and width of stability region of flat flame in terms of acoustic velocity forcing is obtained. Here, the stability region width, *SRW* is defined as difference between minimum acoustic velocity for parametric instability regime and maximum acoustic velocity for hydrodynamic instability regime

$$SRW_{theory} = Ua_{\min\_parametric} - Ua_{\max\_hydrodynamic} \quad (15)$$

SRW can be defined similarly in experiments and its measurement can be done by measuring the acoustic velocity at onset of parametric instability and at termination of hydrodynamic instability (formation of flat flame structure) and taking the difference. In present experiments, *SRW* is not measured explicitly. Such

measurements using an LDV probe was made earlier by Aldredge and Killingsworth (A&K) [16].They measured axial acoustic velocity fluctuations for methane/air flames at saturation of primary instability, $Ua_{\max\_hydrodynamic}$ and at the onset of parametric instability $Ua_{\min\_parametric}$ using LDV and compared with calculations using Bychkov's [29] analysis. However, the analytical predictions were not qualitatively consistent with measurements over the range of equivalence ratios. Here, we calculate *SRW* using their data and compare with $SRW_{corrected}$, (introduced later) calculated using numerical method presented in section 3 as is shown in Fig. 9. The predictions for *SRW* are qualitatively consistent with the measurements. Hence, even though $Ua_{\max\_hydrodynamic}$ and $Ua_{\min\_parametric}$ were not qualitatively consistent with experiments, their difference agrees qualitatively with experiments. Numerical method shows some quantitative improvement over the analytical method used in [16]. The *SRW* in experiments is consistently higher than theoretical values for all equivalence ratios which can be attribute to the small gap annular geometry of experiments where acoustic losses lead to higher stability and thus higher *SRW*. For calculating *SRW* for methane/air flames, we use the transport properties calculated using CHEMKIN; S_L and β is calculated using USC II mechanism.

It should be noted that a direct comparison of critical S_L with measurement of [16] is not possible because regime V was not observed in their work, so, a critical S_L could not be found due to geometry effects discussed in last section. However, the comparison in Fig. 9 shows that the variation of *SRW* with S_L is consistent between experiments and theory. Thus, theoretical results for *SRW* is representative of experiments even though we don't necessarily measure *SRW* and can be successfully used to predict critical S_L. Moreover, measurement of *SRW* is not needed to predict critical S_L.

In theory, critical S_L is the S_L at which width of stability region, *SRW* should become zero i.e. for any value of acoustic forcing, there is a wavenumber or a range of wavenumber which is unstable. However, in experiments, it is possible that a flat flame cannot be observed if the *SRW* is very low. This is because the acoustic forcing continuously increases in experiments and the small range of acoustic forcing

necessary for flat flame formation is not active for sufficient time interval. A negative width of stability region is of no specific physical meaning and it was taken as zero in a previous work [31]. However, here we allow it to assume negative values for reasons which will be clear until the end of this section.

Figure 10 shows the *SRW* at various S_L for all three fuels used in this work. Experimental values of critical S_L are also shown for each *Le* as vertical lines. These calculations are qualitatively consistent with experimental observations. The width of stability region decreases as S_L increases for all *Le* in line with experimental observation that it is easier to transition to parametric instability at higher S_L. Also, *SRW* decreases more rapidly with S_L at lower S_L. for mixtures with *Le* close to unity *SRW* becomes almost constant after a certain S_L. The width of stability region is larger for higher *Le* at similar S_L for all three fuels explaining the experimental fact that critical S_L is higher for higher *Le* for all three fuels. However, quantitative agreement could not be obtained with experiments. Theoretical calculation shows that flat flame cannot be achieved for *Le* ~ 0.76 (CH_4), *Le* ~ 0.80 (C_2H_4) and *Le* ~ 0.78 (C_3H_8) as the stability width is negative even for S_L =10 cm/s. But, flat flame can be observed under such mixture conditions in regime II and III (see Fig. 5). Similarly, for higher than unity *Le* the stability region width doesn't become negligible for *Le* ~ 1.11 (CH_4), *Le* ~ 1.34 (C_2H_4) and *Le* ~ 1.86 (C_3H_8) even at higher S_L where regime V is observed in experiments (see Fig. 5). Interestingly, the theory appears to be in satisfactory quantitative agreement for *Le* near unity as the width of stability region becomes very less for *Le* ~ 0.96 (CH_4), *Le* ~ 1.05, 1.06 (C_2H_4) and *Le* ~ 1.03 (C_3H_8) near experimental critical S_L. This indicates that stability region width and thus critical S_L is overpredicted for *Le* higher than unity and underpredicted for *Le* lower than unity by the theory.

However, Searby and Rochwerger [28] satisfactorily predicted the acoustic velocity and wavenumbers of flame cells at the onset of parametric instability for C_3H_8/air flames using this theory. Hence, it is important to investigate the reasons behind worse predictions of critical S_L in current work. There can be

two possible reasons for such predictions. First, measured value of *Ma* for lean C_3H_8/air mixtures was used in [28], but we used a theoretical estimate of *Ma* using Eqn. 7 for present mixtures because measured values are not available for all mixtures. This theoretical estimate is not accurate, particularly for non-unity *Le* mixtures. For e.g. for lean $C_3H_8/O_2/N_2$ mixtures Eqn. 7 predicts *Ma* of 8.5 but a value of 4.5±0.5 is used in [28]. Second, they [28] worked with the mixtures for which the two regions of instability were well separated, but we are applying it to conditions where both regions of instability merge (definition for critical S_L) and non-linearity of hydrodynamic instability is stronger. Hence, the theory was tested and proved only for acoustic velocity at the onset of parametric instability, $Ua_{\min\_parametric}$, where flame was flat prior to onset of parametric instability, but to correctly predict *SRW*, $Ua_{\max\_hydrodynamic}$ also needs to be correctly predicted (see Eqn. 15). It is observed that at the onset of regime V, the initial curved flame is very non-linear (various cusp formations are observed). Acoustic velocity required to completely suppress these non-linear hydrodynamic instabilities may not be accurately predicted using the theory which accounts only for weak non-linearity. It is essential to quantify the relative importance of these two factors.

First, the effect of *Ma* prediction is assessed by considering the lean $C_3H_8/O_2/N_2$ mixture which is similar to the lean C_3H_8/air mixtures used by [28] with *Ma* of 4.5±0.5. Some change in the ratio O_2/N_2 is not expected to change *Ma* significantly. SRW is calculated with *Ma* of 4.5 and 5.0 and compared with SRW calculated with *Ma* from Eqn. 7 in Fig. 11. It is seen that if measured value of *Ma* is used, the critical S_L can be correctly predicted. This also establishes that effect of non-linearity is of limited significance in calculating the critical S_L and stability boundary can be successfully studied using the linear theory even for the mixtures where both instability regimes are closer, if the correct value of *Ma* is known. Conversely, if critical S_L is measured, *Ma* can be estimated using this theory. In past, measurement of $Ua_{\min\_parametric}$ and $Ua_{\max\_hydrodynamic}$ had also been used to estimate *Ma* [30].

To make better quantitative predictions for other conditions where measured value of *Ma* is not known, a correction factor can be proposed. It is evident from Fig. 10 that theoretical prediction of stability region width should be corrected for *Le* effect by employing a correction term which should be function of *Le*. Also, the function should return zero for *Le* =1, reduce the stability width for *Le* >1 and increase the stability width for *Le* <1. In this work, we propose a function of form $F = n * (Le - 1)/Le$, where n is an unknown constant. So, the corrected stability region width, $SRW_{corrected}$ is given by

$$SRW_{corrected} = SRW_{theory} - n(Le - 1)/Le \qquad (16)$$

Where, SRW_{theory} is theoretical value of stability region width. If we assume $n \approx 6$, it significantly improves the agreements between experiments and theory for critical S_L. To explain the significance of $n \approx 6$, we note that $\frac{1}{2}\beta \approx 6$ for presented hydrocarbon flames. Hence, the modified form of (16) can be written as

$$SRW_{corrected} = SRW_{theory} - \frac{1}{2}\beta(Le - 1)/Le \qquad (17)$$

Figure 11 shows the stability width after applying the correction factor from Eqn. 17 for lean $C_3H_8/O_2/N_2$ mixtures and it is observed that $SRW_{corrected}$ lies between SRW calculated from *Ma* of 4.5 and 5.0 near critical S_L. This means that the correction factor proposed in current work mainly acts as a correction for *Ma*. Figure 12 shows $SRW_{corrected}$ calculated for all the mixtures used in this work. Obviously, stability width reduces for larger than unity and increases for lower than unity. The predictions for critical S_L now show good agreement with experiments. Interestingly, this simple correction factor is very effective as it can improve predictions of critical S_L irrespective of *Le* and fuel.

Conclusions

Effect of *Le* on transition to "complete instability" (where no flat flame is observed) is studied experimentally and theoretically in thermo-acoustically unstable downward propagating flames. Lowest S_L of mixture for which complete instability is observed is termed "critical S_L". Higher *Le* flames showed higher critical S_L for any fuel. Theoretical calculations successfully captured the effect of *Le*. Much better quantitative agreement between experiments and theory is obtained by applying a correction factor which is a function of β and *Le*. The correction factor acts as a correction for *Ma*. The measurement of "critical S_L" can also be used to estimate *Ma*.

Acknowledgements

This study was supported by a Grant-in-Aid for Scientific Researches (KIBAN(A)#18H03755) from MEXT Japan.

Appendix

Mixture	CH_4	O_2	N_2	Φ	D (cm^2/s)	S_L (cm/s)	T_b (K)	ρ_u (g/cm3)	ρ_b (g/cm3)	*Le*	Regime	*Ma*	β
1	0.063	0.158	0.778		0.22203	12.5	1743	0.00114	0.000195	0.969	I		13.24
2	0.066	0.165	0.769		0.22208	15.0	1796	0.00114	0.000189	0.967	II	4.1248	13.21
3	0.069	0.172	0.760		0.22212	17.5	1843	0.001139	0.000184	0.966	III		13.00
4	0.071	0.178	0.751		0.22216	20.0	1886	0.001139	0.00018	0.965	III	4.2878	12.67
5	0.073	0.183	0.743		0.22219	22.5	1926	0.001139	0.000176	0.964	IV		12.59
6	0.076	0.189	0.736		0.22223	25.0	1963	0.001139	0.000173	0.964	IV	4.4247	12.51
7	0.078	0.194	0.728		0.22226	27.5	1998	0.001139	0.00017	0.963	IV		12.56
8	0.080	0.199	0.721	0.8	0.22229	30.0	2032	0.001138	0.000167	0.962	IV	4.536	12.66
9	0.082	0.204	0.714		0.22232	32.5	2062	0.001138	0.000164	0.961	V	4.5857	12.66
10	0.083	0.208	0.708		0.22235	35.0	2090	0.001138	0.000162	0.96	V	4.6299	12.70
11	0.085	0.213	0.702		0.22238	37.5	2118	0.001138	0.00016	0.96	V	4.6809	12.73
12	0.087	0.218	0.695		0.2224	40.0	2145	0.001138	0.000158	0.959	V	4.7187	12.97
13	0.091	0.227	0.682		0.22246	45.0	2195	0.001138	0.000154	0.957	VI		13.20
14	0.094	0.236	0.670		0.22251	50.0	2238	0.001137	0.000151	0.956	VI		13.35
15	0.098	0.245	0.656		0.22257	55.75	2287	0.001137	0.000147	0.954	VI		13.57
16	0.092	0.153	0.755		0.22256	15.0	1879	0.001125	0.000173	1.097	I	5.1084	15.62
17	0.095	0.158	0.747	1.2	0.22261	17.5	1918	0.001124	0.000169	1.099	I		14.58
18	0.098	0.163	0.740		0.22266	20.0	1953	0.001124	0.000166	1.1	III	5.1837	13.71

19	0.100	0.167	0.733		0.22270	22.5	1987	0.001123	0.000163	1.101	IV		13.09
20	0.103	0.171	0.726		0.22274	25.0	2021	0.001123	0.00016	1.102	IV	5.2718	12.63
21	0.105	0.175	0.719		0.22278	27.5	2055	0.001122	0.000157	1.105	IV		12.28
22	0.108	0.180	0.713		0.22283	30.0	2086	0.001122	0.000154	1.105	IV	5.3785	12.09
23	0.110	0.184	0.706		0.22287	32.5	2117	0.001121	0.000152	1.106	IV	5.4256	11.81
24	0.113	0.188	0.699		0.22291	35.0	2147	0.00112	0.00015	1.107	IV	5.4775	11.69
25	0.114	0.190	0.696		0.22293	35.25	2161	0.00112	0.000149	1.108	IV		11.71
26	0.115	0.192	0.693		0.22295	37.5	2175	0.00112	0.000147	1.108	V	5.5302	11.62
27	0.132	0.220	0.649		0.22322	55.0	2350	0.001116	0.000135	1.117	V		12.14
Mixture	CH_4	O_2	CO_2	Φ	D (cm^2/s)	S_L (cm/s)	T_b (K)	ρ_u (g/cm3)	ρ_b (g/cm3)	*Le*	Regime	*Ma*	β
28	0.095	0.237	0.668	0.8	0.14228	7.5	1798	0.001574	0.000261	0.74	II		13.06
29	0.100	0.251	0.648		0.14419	10.0	1878	0.001561	0.000247	0.744	II	3.4374	13.08
30	0.106	0.264	0.630		0.14593	12.5	1946	0.001549	0.000237	0.747	III	3.5829	13.17
31	0.110	0.275	0.615		0.14745	15.0	2002	0.001538	0.000228	0.75	IV	3.6774	13.51
32	0.114	0.285	0.601		0.14886	17.5	2050	0.001529	0.000221	0.753	V	3.7759	13.65
33	0.118	0.294	0.588		0.15019	20.0	2093	0.001520	0.000215	0.756	V	3.8423	14.00
34	0.121	0.303	0.576		0.15143	22.5	2133	0.001511	0.000210	0.758	V		14.51
35	0.125	0.311	0.564		0.15261	25.0	2167	0.001504	0.000205	0.76	VI		15.15
36	0.128	0.319	0.553		0.15373	27.5	2196	0.001496	0.000201	0.762	VI		15.12
37	0.131	0.327	0.543		0.15484	30.0	2226	0.001489	0.000197	0.765	VI		15.67
38	0.144	0.360	0.496		0.15980	42.5	2338	0.001458	0.000182	0.774	VI		17.06
39	0.133	0.222	0.645	1.2	0.14518	7.5	1898	0.001538	0.000231	0.854	II		13.66
40	0.141	0.235	0.625		0.14721	10.0	1979	0.001523	0.000219	0.862	III	4.4339	12.53
41	0.147	0.245	0.609		0.14884	12.5	2044	0.001511	0.000210	0.868	IV	4.587	12.68
42	0.153	0.254	0.593		0.15040	15.0	2102	0.001500	0.000202	0.874	IV	4.7311	12.74
43	0.158	0.263	0.580		0.15179	17.5	2150	0.001490	0.000196	0.88	IV	4.8409	13.03
44	0.163	0.271	0.567		0.15317	20.0	2194	0.001480	0.000190	0.885	V	4.9201	13.74
45	0.167	0.278	0.555		0.15444	22.5	2234	0.001471	0.000185	0.89	V		14.36
46	0.171	0.286	0.543		0.15566	25.0	2268	0.001463	0.000181	0.895	V	5.0797	14.63
47	0.175	0.292	0.532		0.15680	27.5	2299	0.001455	0.000177	0.9	V		15.18
48	0.179	0.299	0.522		0.15797	30.0	2328	0.001447	0.000174	0.905	VI		15.84
49	0.183	0.305	0.512		0.15899	32.5	2351	0.001440	0.000170	0.909	VI		16.12
50	0.187	0.311	0.502		0.16005	35.0	2374	0.001433	0.000168	0.914	VI		16.68
Mixture	C_2H_4	O_2	N_2	Φ	D (cm^2/s)	S_L (cm/s)	T_b (K)	ρ_u (g/cm3)	ρ_b (g/cm3)	*Le*	Regime	*Ma*	β
51	0.036	0.135	0.829	0.8	0.21470	15.0	1692	0.001167	0.000206	1.35	I		11.83
52	0.038	0.141	0.821		0.21444	17.5	1742	0.001168	0.000200	1.348	I		11.57
53	0.039	0.147	0.814		0.21419	20.0	1787	0.001169	0.000195	1.346	III		11.31
54	0.040	0.151	0.808		0.21396	22.5	1830	0.001170	0.000190	1.345	III		11.23
55	0.042	0.156	0.802		0.21375	25.0	1869	0.001171	0.000187	1.343	III	5.965	11.10
56	0.043	0.161	0.796		0.21353	27.5	1908	0.001171	0.000183	1.342	IV		11.09
57	0.044	0.166	0.790		0.21332	30.0	1944	0.001172	0.000180	1.341	IV	6.0495	10.88
58	0.045	0.170	0.785		0.21312	32.5	1978	0.001173	0.000177	1.34	III		10.75
59	0.046	0.174	0.779		0.21293	35.0	2012	0.001173	0.000174	1.338	III	6.1333	10.77

60	0.048	0.178	0.774		0.21273	37.5	2044	0.001174	0.000171	1.337	V	6.214	11.02
61	0.045	0.112	0.843	1.2	0.21325	10.0	1651	0.001163	0.000205	1.062	I		15.41
62	0.047	0.117	0.836		0.21293	12.5	1698	0.001164	0.000199	1.062	II		14.33
63	0.049	0.121	0.830		0.21263	15.0	1742	0.001165	0.000194	1.061	III	4.5483	13.46
64	0.050	0.126	0.824		0.21233	17.5	1786	0.001166	0.000189	1.061	IV		12.80
65	0.052	0.130	0.818		0.21206	20.0	1825	0.001166	0.000185	1.061	IV	4.6642	12.08
66	0.054	0.134	0.813		0.21179	22.5	1864	0.001167	0.000181	1.061	IV		11.64
67	0.055	0.138	0.807		0.21153	25.0	1902	0.001168	0.000178	1.061	IV	4.7849	11.38
68	0.057	0.142	0.802		0.21126	27.5	1940	0.001168	0.000174	1.061	IV	4.8478	11.22
69	0.058	0.145	0.796		0.21102	30.0	1975	0.001169	0.000171	1.061	V	4.9056	11.07
70	0.060	0.149	0.791		0.21077	32.5	2008	0.001169	0.000168	1.061	V		10.77
71	0.061	0.153	0.786		0.21054	35.0	2040	0.001170	0.000165	1.061	V	5.0067	10.47
72	0.062	0.156	0.781		0.21030	37.5	2074	0.001171	0.000163	1.061	V		10.54
73	0.064	0.160	0.776		0.21006	40.0	2106	0.001171	0.000160	1.061	V	5.1192	10.36
74	0.065	0.163	0.771		0.20983	42.5	2136	0.001172	0.000158	1.061	V		10.44
75	0.067	0.167	0.767		0.20960	45.0	2165	0.001172	0.000156	1.061	V		10.23
76	0.068	0.170	0.762		0.20938	47.5	2192	0.001173	0.000154	1.061	V		10.44
Mixture	C_2H_4	O_2	CO_2	Φ	D (cm^2/s)	S_L (cm/s)	T_b (K)	ρ_u (g/cm3)	ρ_b (g/cm3)	Le	Regime	Ma	β
77	0.051	0.190	0.759	0.8	0.12798	7.5	1626	0.001673	0.000307	1.042	I		12.01
78	0.054	0.204	0.741		0.12912	10.0	1717	0.001663	0.000289	1.045	II		11.74
79	0.057	0.216	0.727		0.13002	12.5	1787	0.001656	0.000276	1.048	II		11.59
80	0.060	0.226	0.714		0.13084	15.0	1850	0.001649	0.000265	1.05	III	5.1291	11.70
81	0.063	0.236	0.702		0.13163	17.5	1907	0.001642	0.000256	1.052	III		11.96
82	0.065	0.244	0.690		0.13235	20.0	1957	0.001636	0.000249	1.054	III		12.25
83	0.067	0.253	0.680		0.13304	22.5	2002	0.001631	0.000242	1.056	V	5.4734	12.67
84	0.070	0.261	0.670		0.13368	25.0	2042	0.001626	0.000236	1.057	V	5.5593	12.91
85	0.070	0.176	0.754	1.2	0.12677	7.5	1707	0.001667	0.000281	0.78	II		12.78
86	0.075	0.186	0.739		0.12759	10.0	1786	0.001659	0.000266	0.79	II	3.6846	12.23
87	0.079	0.196	0.725		0.12837	12.5	1858	0.001651	0.000254	0.79	III	3.8938	11.83
88	0.082	0.205	0.713		0.12906	15.0	1922	0.001645	0.000245	0.79	IV	4.0336	11.90
89	0.085	0.213	0.701		0.12971	17.5	1982	0.001638	0.000236	0.80	V	4.1646	12.01
90	0.089	0.222	0.690		0.13035	20.0	2036	0.001632	0.000228	0.80	V		12.19
91	0.091	0.229	0.680		0.13092	22.5	2084	0.001627	0.000222	0.80	VI	4.3463	12.63
92	0.094	0.236	0.670		0.13146	25.0	2128	0.001623	0.000216	0.80	VI	4.4256	12.94
93	0.097	0.242	0.661		0.13201	27.5	2167	0.001617	0.000211	0.80	VI	4.5128	13.00
94	0.099	0.249	0.652		0.13252	30.0	2204	0.001612	0.000207	0.81	VI	4.5143	14.02
Mixture	C_3H_8	O_2	N_2	Φ	D (cm^2/s)	S_L (cm/s)	T_b (K)	ρ_u (g/cm3)	ρ_b (g/cm3)	Le	Regime	Ma	β
95	0.027	0.169	0.804	0.8	0.20813	17.5	1833	0.001190	0.000188	1.871	I		11.27
96	0.028	0.175	0.797		0.20764	20.0	1881	0.001192	0.000184	1.868	I	8.2508	11.20
97	0.029	0.182	0.789		0.20716	22.5	1927	0.001194	0.000179	1.865	I		11.29
98	0.030	0.188	0.782		0.20673	25.0	1969	0.001195	0.000175	1.862	II		11.42
99	0.031	0.194	0.775		0.20631	27.5	2009	0.001197	0.000172	1.859	IV		11.47
100	0.032	0.200	0.768		0.20586	30.0	2046	0.001199	0.000169	1.857	IV	8.4844	11.41

101	0.033	0.206	0.762		0.20546	32.5	2082	0.001200	0.000166	1.854	III		11.52
102	0.034	0.211	0.755		0.20508	35.0	2114	0.001202	0.000163	1.851	III		11.62
103	0.035	0.217	0.749		0.20468	37.5	2145	0.001203	0.000161	1.849	III		11.68
104	0.035	0.222	0.743		0.20432	40.0	2175	0.001204	0.000159	1.846	V	8.8277	11.85
105	0.033	0.135	0.832		0.20571	7.5	1705	0.001188	0.000195	1.041	II		17.73
106	0.034	0.142	0.823		0.20497	10.0	1761	0.001191	0.000189	1.04	II	4.458	15.83
107	0.036	0.149	0.816		0.20431	12.5	1812	0.001193	0.000183	1.039	III		14.40
108	0.037	0.155	0.808		0.20368	15.0	1859	0.001195	0.000179	1.038	III	4.583	13.67
109	0.039	0.161	0.801		0.20306	17.5	1905	0.001196	0.000174	1.037	IV		12.87
110	0.040	0.166	0.794		0.20248	20.0	1948	0.001198	0.000170	1.036	IV	4.7079	12.45
111	0.041	0.172	0.787		0.20190	22.5	1990	0.001200	0.000166	1.035	IV	4.7653	11.82
112	0.042	0.177	0.781	1.2	0.20135	25.0	2030	0.001202	0.000163	1.034	V	4.826	11.69
113	0.044	0.182	0.774		0.20082	27.5	2067	0.001203	0.000160	1.034	V		11.45
114	0.045	0.187	0.768		0.20028	30.0	2104	0.001205	0.000157	1.033	V	4.9396	11.16
115	0.046	0.192	0.761		0.19977	32.5	2139	0.001207	0.000154	1.032	VI		11.22
116	0.047	0.197	0.755		0.19925	35.0	2175	0.001208	0.000151	1.031	VI	5.0486	11.20
117	0.049	0.202	0.749		0.19876	37.5	2206	0.001210	0.000149	1.031	VI		11.01
118	0.050	0.207	0.743		0.19825	40.0	2238	0.001212	0.000147	1.03	VI		10.96
119	0.051	0.212	0.737		0.19776	42.5	2268	0.001213	0.000145	1.029	VI		10.95
Mixture	C_3H_8	O_2	CO_2	Φ	D (cm^2/s)	S_L (cm/s)	T_b (K)	ρ_u (g/cm3)	ρ_b (g/cm3)	Le	Regime	Ma	β
120	0.039	0.246	0.715		0.12689	10.0	1825	0.001678	0.000263	1.482	I	7.1663	11.56
121	0.042	0.261	0.697		0.12772	12.5	1901	0.001671	0.000251	1.485	III		11.21
122	0.044	0.273	0.683		0.12839	15.0	1965	0.001665	0.000241	1.487	IV	7.3922	11.46
123	0.046	0.285	0.669	0.8	0.12907	17.5	2022	0.001659	0.000233	1.489	IV		12.17
124	0.047	0.297	0.656		0.12972	20.0	2071	0.001653	0.000226	1.491	III	7.8672	12.93
125	0.049	0.307	0.644		0.13030	22.5	2115	0.001648	0.000220	1.493	V	8.0752	13.60
126	0.051	0.317	0.632		0.13088	25.0	2153	0.001643	0.000214	1.495	V	8.1995	13.92
127	0.054	0.227	0.719		0.12332	7.5	1848	0.001688	0.000246	0.77	II		12.29
128	0.058	0.242	0.700		0.12395	10.0	1939	0.001680	0.000232	0.773	III	3.9993	11.75
129	0.061	0.254	0.684		0.12449	12.5	2013	0.001674	0.000222	0.775	V	4.1614	11.74
130	0.064	0.266	0.670		0.12498	15.0	2080	0.001668	0.000213	0.777	V	4.2861	11.95
131	0.067	0.278	0.656		0.12548	17.5	2138	0.001663	0.000205	0.778	VI	4.3269	12.87
132	0.069	0.289	0.642	1.2	0.12595	20.0	2188	0.001657	0.000199	0.78	VI	4.4234	13.03
133	0.072	0.299	0.630		0.12637	22.5	2233	0.001653	0.000193	0.782	VI		13.48
134	0.074	0.308	0.618		0.12678	25.0	2271	0.001648	0.000188	0.784	VI		14.13
135	0.076	0.318	0.606		0.12719	27.5	2307	0.001643	0.000184	0.785	VI		14.96
136	0.078	0.326	0.596		0.12755	30.0	2337	0.001639	0.000180	0.787	VI		15.83
137	0.080	0.334	0.586		0.12790	32.5	2365	0.001635	0.000177	0.789	VI		16.53

References

[1] T. C. Lieuwen, *Unsteady Combustor Physics*, (2012) . Cambridge: Cambridge University Press, 2012.

[2] T. Poinsot, Prediction and control of combustion instabilities in real engines, Proc. Combust. Inst., 36 (2017) , 1–28.

[3] J. W. S. B. Rayleigh, The explanation of certain acoustical phenomena 1, Nature, 18 (1878) , 319–321.

[4] G. Searby, Acoustic Instability in Premixed Flames, Combust. Sci. Technol., 81 (1992) , 221–231.

[5] P. Clavin, Dynamic behavior of premixed flame fronts in laminar and turbulent flows, Prog. Energy Combust. Sci., 11 (1985) , 1–59.

[6] P. Clavin, P. Pelcé, L. He, One-dimensional vibratory instability of planar flames propagating in tubes, J. Fluid Mech., 216 (1990) , 299-322.

[7] A. C. Mcintosh, Pressure disturbances of Different Length Scales Interacting with Conventional Flames, Combust. Sci. Technol., 75 (1991) , 287–309.

[8] P. Clavin, G. Searby, Unsteady response of chain-branching premixed-flames to pressure waves, Combust. Theory Model., 12 (2008) , 545–567.

[9] P. Pelcé, D. Rochwerger, Vibratory instability of cellular flames propagating in tubes, J. Fluid Mech., 239 (1992) , 293–307.

[10] X. Wu, M. Wang, P. Moin, N. Peters, Combustion instability due to the nonlinear interaction between sound and flame, J. Fluid Mech., 497 (2003), 23-53.

[11] R. C. Assier, X. Wu, Linear and weakly nonlinear instability of a premixed curved flame under the influence of its spontaneous acoustic field, J. Fluid Mech, 758 (2017) , 180–220.

[12] A. K. Dubey, Y. Koyama, N. Hashimoto, O. Fujita, Effect of geometrical parameters on thermo-acoustic instability of downward propagating flames in tubes, Proc. Combust. Inst., 37 (2019) 1869-1877.

[13] A. K. Dubey, Y. Koyama, N. Hashimoto, O. Fujita, Experimental and theoretical study of secondary acoustic instability of downward propagating flames: higher modes and growth rates, Combust. Flame, 205 (2019) , 316–326.

[14] C. Clanet, G. Searby, P. Clavin, Primary acoustic instability of flames propagating in tubes: cases of spray and premixed gas combustion, J. Fluid Mech., 385 (1999) , 157–197.

[15] V. Vaezi, R.C . Aldredge, Laminar-flame instabilities in a taylor-couette combustor, Combust. Flame, 121 (2000) , 356–366.

[16] R. C. Aldredge, N. J. Killingsworth, Experimental evaluation of Markstein-number influence on thermoacoustic instability, Combust. Flame, 137 (2004) , 178–197.

[17] V. Vaezi and R. C. Aldredge, Influences of acoustic instabilities on turbulent-flame propagation, Exp. Thermal Fluid Sci., 20 (2000), 162-169.

[18] J. Yáñez, M. Kuznetsov, J. Grune, Flame instability of lean hydrogen-air mixtures in a smooth open-ended vertical channel, Combust. Flame, 162 (2015), 2830-2839.

[19] F. Veiga-López , D. Martínez-Ruiz, E. Fernández-Tarrazo, M. Sánchez-Sanz, Experimental analysis of oscillatory premixed flames in a Hele-Shaw cell propagating towards a closed end, Combust. Flame, 201 (2019) , 1–19.

[20] M. Tsuchimoto, O. Fujita, T. Honko, Y. Nakamura, H. Ito, Research on the relation of flame front

curvature and oscillatory flame propagation by external laser irradiation method, Proc. Combust. Inst., 32 (2009) , 1003–1009.

[21] J. S. Park, O. Fujita, Y. Nakamura, H. Ito, Transition of flat flames to turbulent motion induced by external laser irradiation, Proc. Combust. Inst., 33 (2011) , 1105–1112.

[22] Y. Taniyama, O. Fujita, Initiation and formation of the corrugated structure leading to the self-turbulization of downward propagating flames in a combustion tube with external laser absorption, Combust. Flame, 161 (2014) , 1558–1565.

[23] S. H. Yoon, T. J. Noh, O. Fujita, Onset mechanism of primary acoustic instability in downward-propagating flames, Combust. Flame, 170 (2016) , 1–11.

[24] S. H. Yoon, T. J. Noh, O. Fujita, Effects of Lewis number on generation of primary acoustic instability in downward-propagating flames, Proc. Combust. Inst., 36 (2016) , 1603–1611.

[25] S. H. Yoon, L. Hu, O. Fujita, Experimental observation of pulsating instability under acoustic field in downward-propagating flames at large Lewis number, Combust. Flame, 188 (2018) , 1–4.

[26] Y. Chung, O. Fujita, N. Hashimoto, Effect of Le on criteria of transition to secondary acoustic instability of downward-propagating flame in a tube with controlled curvature induced by external laser, Proc. Combust. Inst., 37 (2019), 1887-1894.

[27] G.H. Markstein, in: G.H. Markstein (Eds.), Non-steady Flame Propagation, Pergamon, New York, 1964, p. 52

[28] G. Searby, D. Rochwerger, A parametric acoustic instability in premixed flames, J. Fluid Mech., 231 (1991) , 529–543.

[29] V. Bychkov, Analytical scalings for flame interaction with sound waves, Phys. Fluids, 11 (1999) , 3168–3173.

[30] R. C. Aldredge, Methane-Air Markstein mumbers from measurements of thermoacoustic instability, Combust. Sci. Technol., 177 (2005), 1023-1047.

[31] J. Yáñez, M. Kuznetsov, R. Redlinger, The acoustic–parametric instability for hydrogen–air mixtures, Combust. Flame, 160 (2013) , 2009–2016.

[32] H. Wang, X. You, A. V. Joshi, S. G. Davis, A. Laskin, F. Egolfopoulos, C. K. Law, USC Mech Version II. High-Temperature combustion reaction model of H2/CO/C1-C4 compounds, http://ignis.usc.edu/USC_Mech_II.htm, May 2007.

[33] G. Searby, P. Clavin, Weakly turbulent, wrinkled flames in premixed gases, Combust. Sci. Technol., 46 (1986) , 167–193.

[34] T. Jones, Mathieu's Equation Solution and Stability, <http://www.physics.drexel.edu/~tim/open/mat/node2.html>.

[35] J.E. Sträng, https://arxiv.org/abs/math-ph/0510076v2

[36] H. Kobayashi, H. Hagiwara, H. Kaneko, Y. Ogami, Effects of CO_2 dilution on turbulent premixed flames at high pressure and high temperature, Proc. Combust. Inst., 31 (2007) , 1451–1458.

[37] J. Lewis, R. Marsh, A. Valera-Medina, S. Morris, H. Baej, The Use of CO_2 to Improve Stability and Emissions of an IGCC Combustor, ASME Turbo Expo 2014: Turbine Technical Conference and Exposition, Düsseldorf, Germany (June 2014) , Paper No. GT2014-25446.

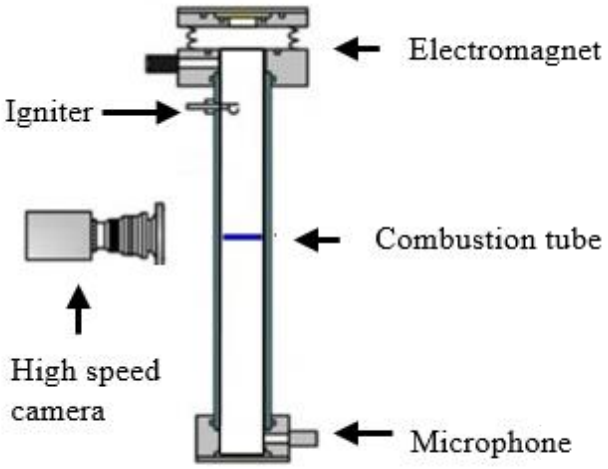

Figure 1. Schematic of experimental setup.

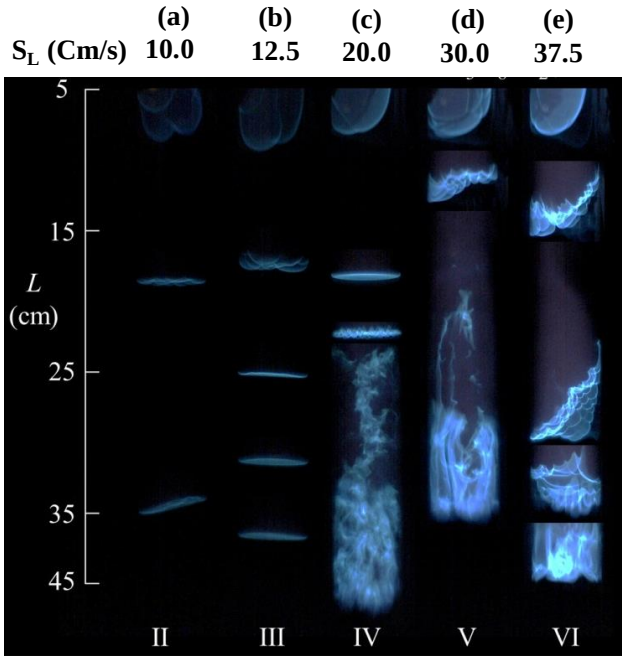

Figure 2. Representative images during flame propagation in regime II to regime VI for $C_3H_8/N_2/O_2$ mixture at equivalence ratio of 1.2. Part of this figure is adapted from our previous works [12, 13, 24, 25].

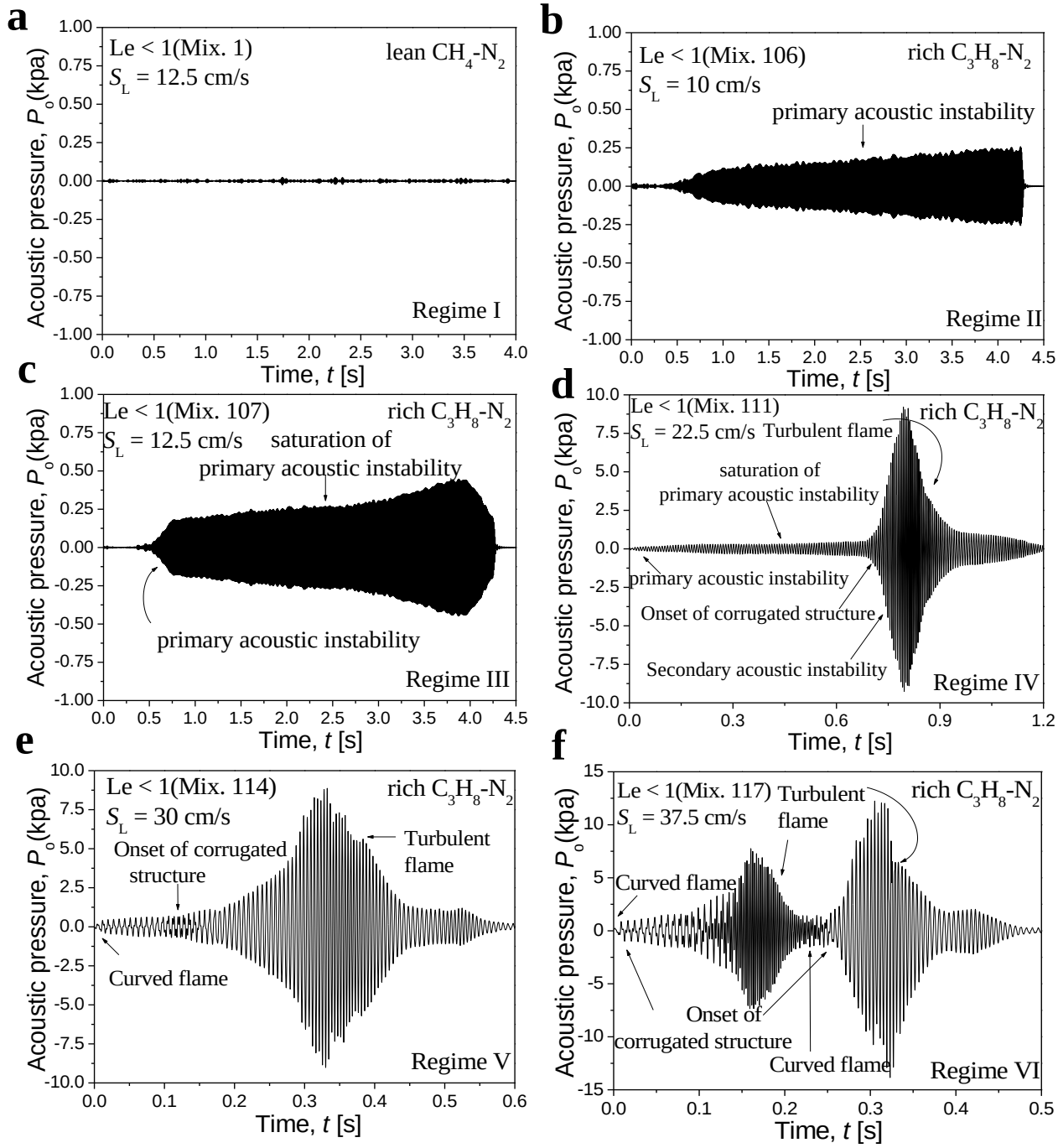

Figure 3. Pressure fluctuations associated with regime I to VI. Similar pressure fluctuation histories were presented earlier for regime III [24], V and VI [13] for non-identical mixtures.

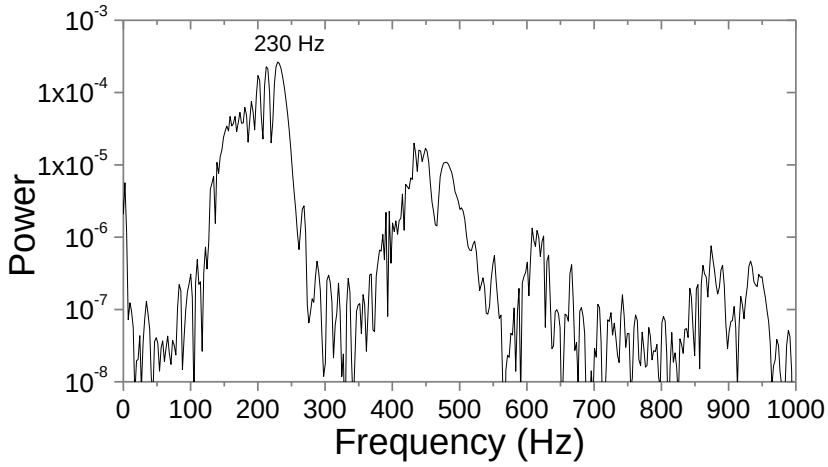

Fig. 4. Frequency spectrum of measured pressure signal for rich $C_3H_8/O_2/N_2$ flame at 22.5 cm/s (regime IV).

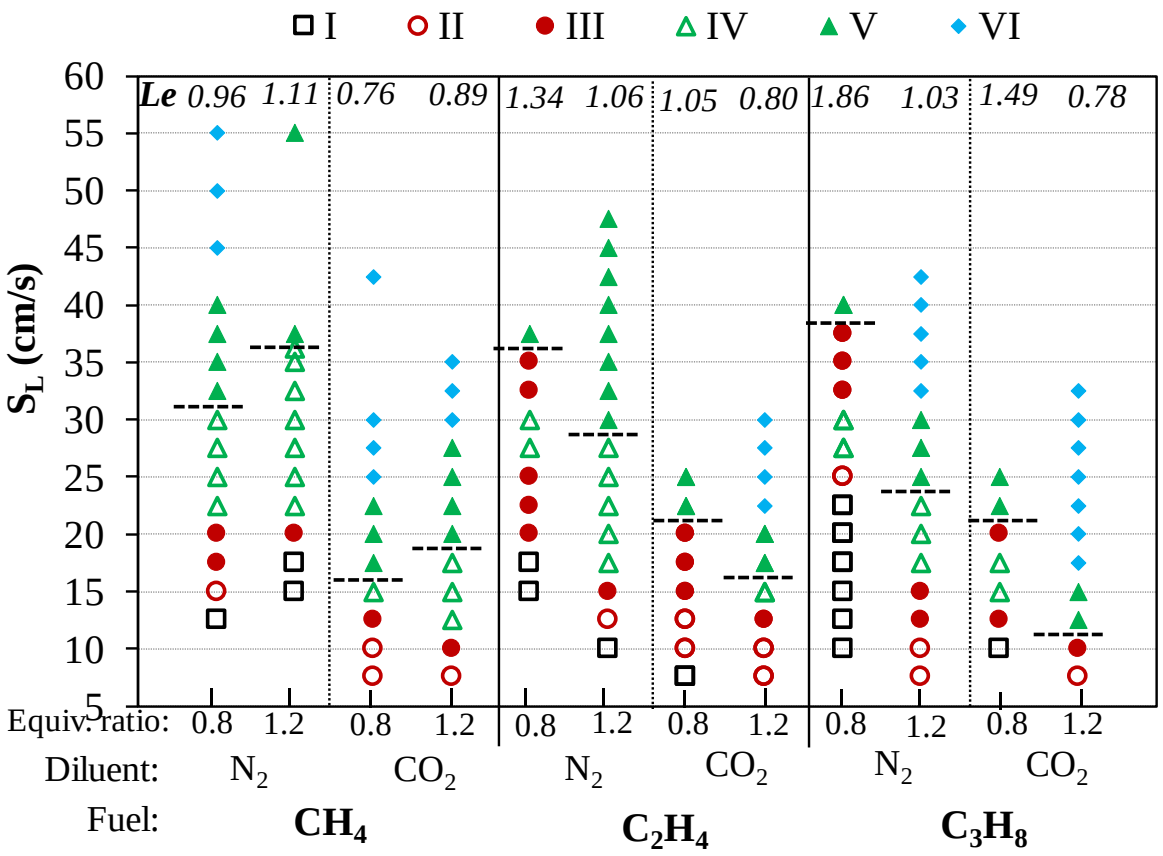

Fig. 5. Summary of flame regimes observed for range of S_L showing effect of fuel, dilution and *Le*. Critical S_L is shown by dashed line for each *Le*.

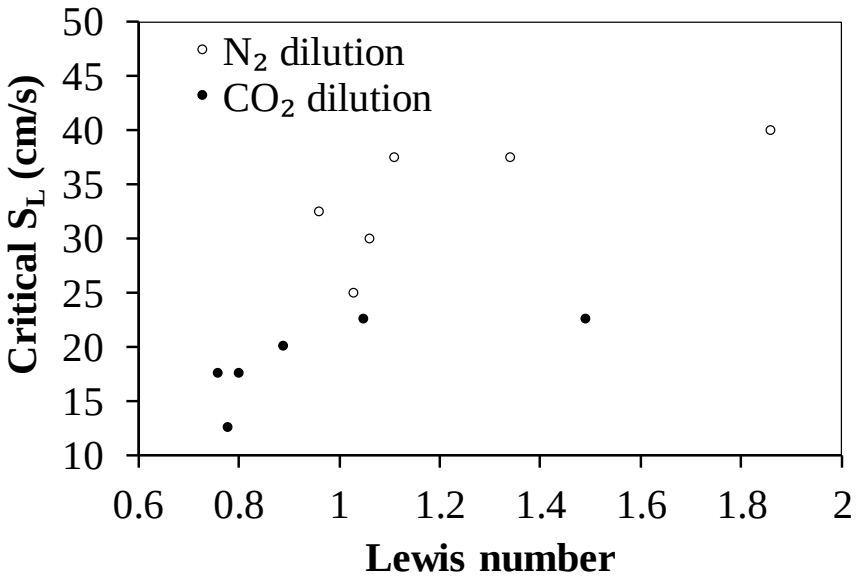

Fig. 6. Comparison of critical S_L for N_2 and CO_2 dilution conditions.

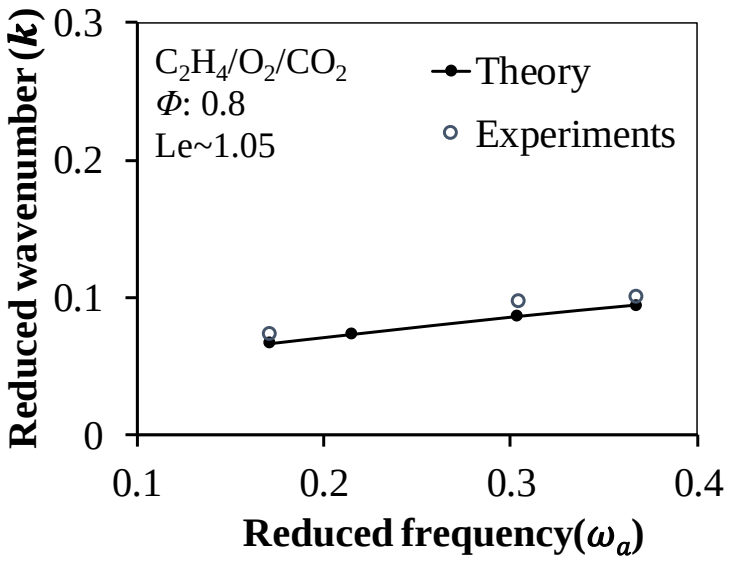

Fig. 7. Wavenumbers at onset of parametric instability

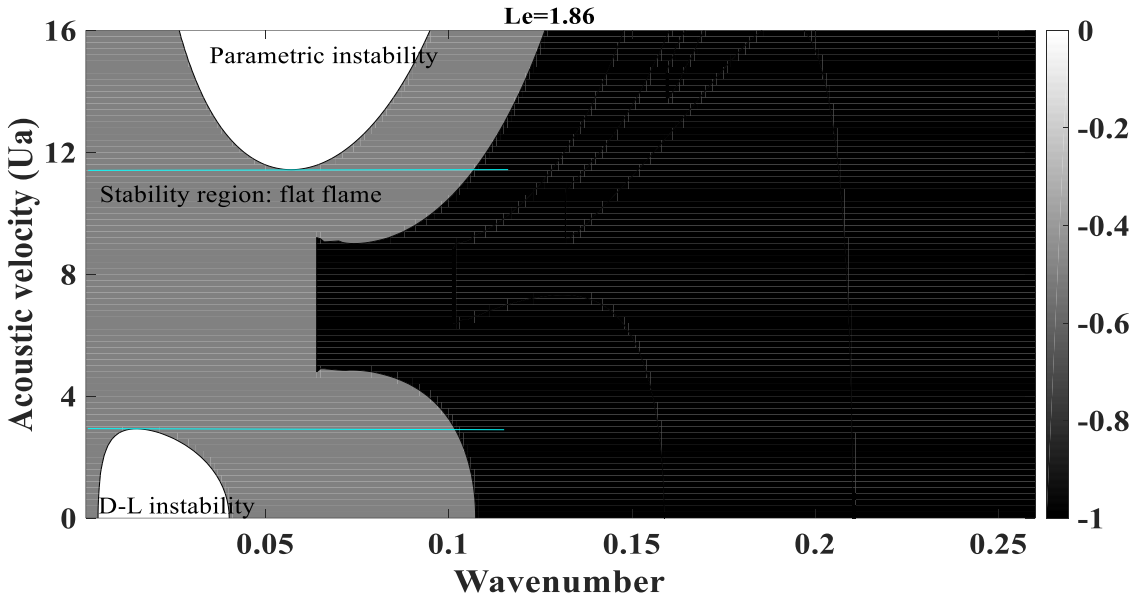
Le=1.86
Parametric instability
Stability region: flat flame
D-L instability
Acoustic velocity (Ua)
Wavenumber
16
12
8
4
0
0.05
0.1
0.15
0.2
0.25
0
-0.2
-0.4
-0.6
-0.8
-1

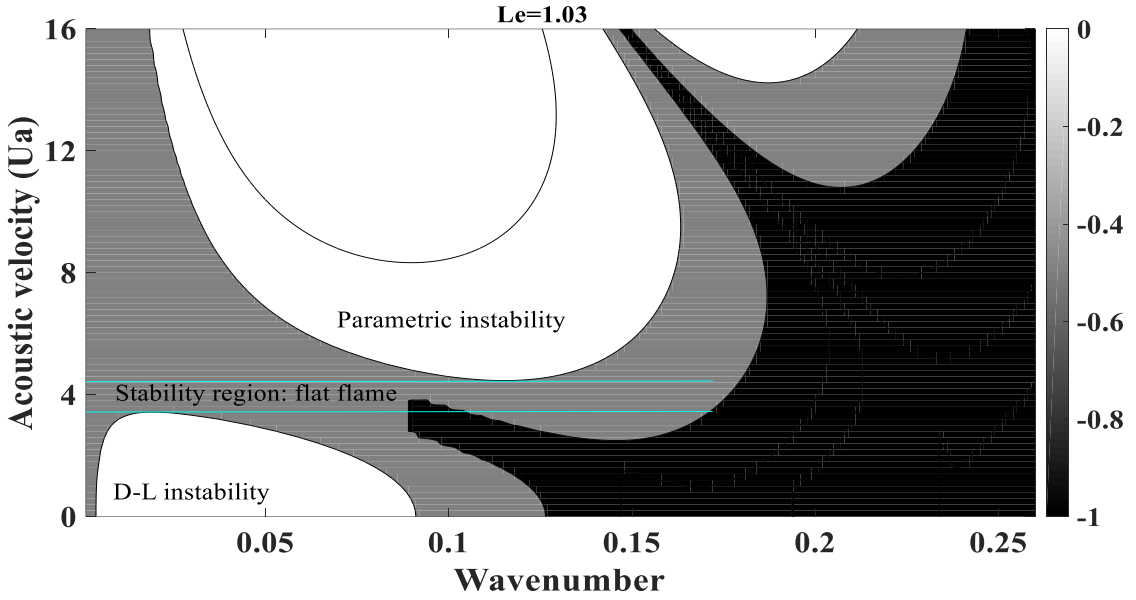
Le=1.03
Parametric instability
Stability region: flat flame
D-L instability
Acoustic velocity (Ua)
Wavenumber
16
12
8
4
0
0.05
0.1
0.15
0.2
0.25
0
-0.2
-0.4
-0.6
-0.8
-1

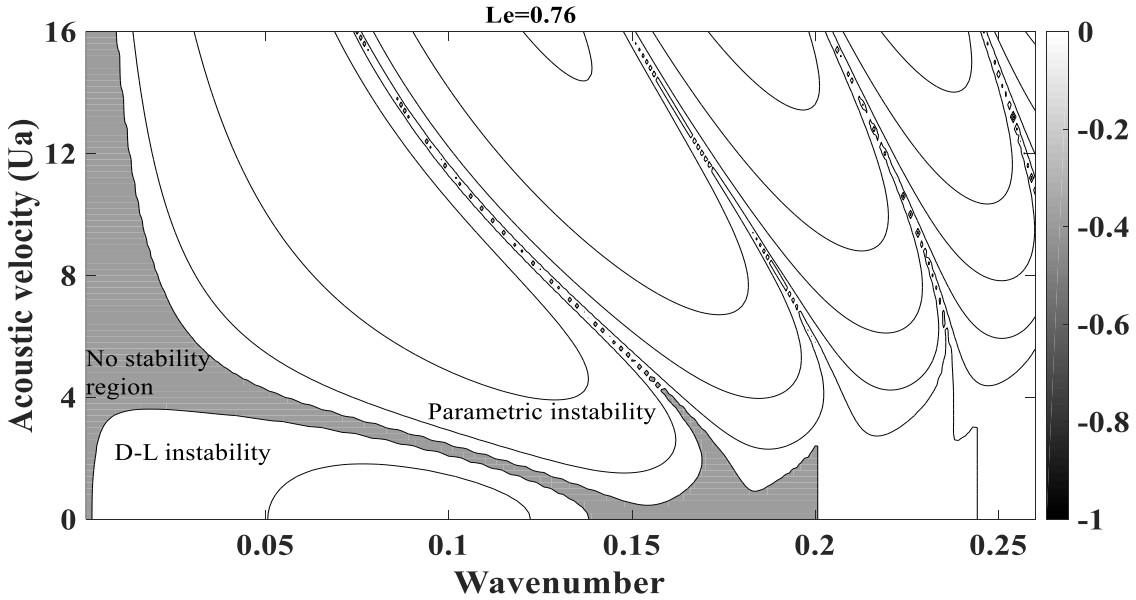
Le=0.76
No stability region
Parametric instability
D-L instability
Acoustic velocity (Ua)
Wavenumber
16
12
8
4
0
0.05
0.1
0.15
0.2
0.25
0
-0.2
-0.4
-0.6
-0.8
-1

Fig. 8. Instability regime diagrams in non-dimensional acoustic velocity and non-dimensional wavenumber plane showing D-L (hydrodynamic) and parametric instability for Le of 1.86 (lean $C_3H_8/O_2/N_2$), 1.03 (rich $C_3H_8/O_2/N_2$) and 0.76 (lean $CH_4/O_2/CO_2$) at a constant S_L of 20 cm/s. Wavenumber is non-dimensionalized by flame thickness, d. Contours are of term F defined in Eqn. 14. Unstable region is shown in white.

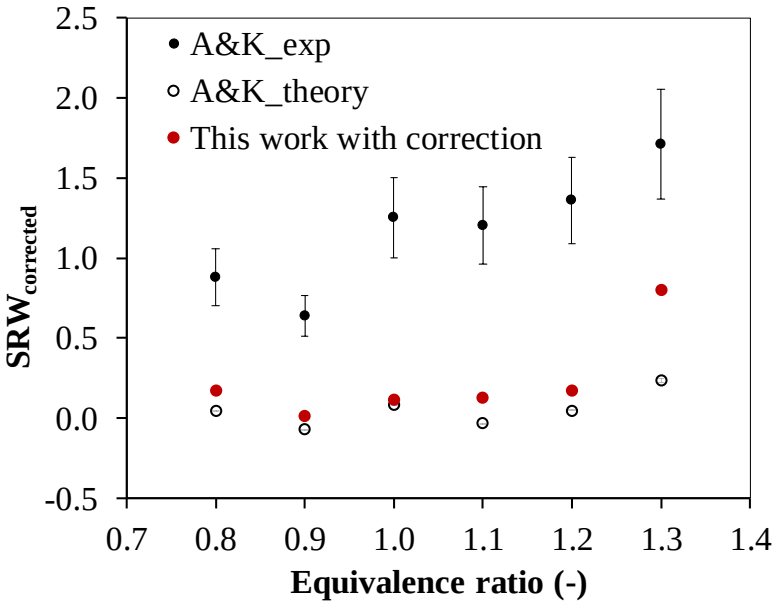

Fig. 9. Stability region width from experiments and theoretical calculation for methane/air flames of A&K [16]. Numerical calculations from this work are also presented.

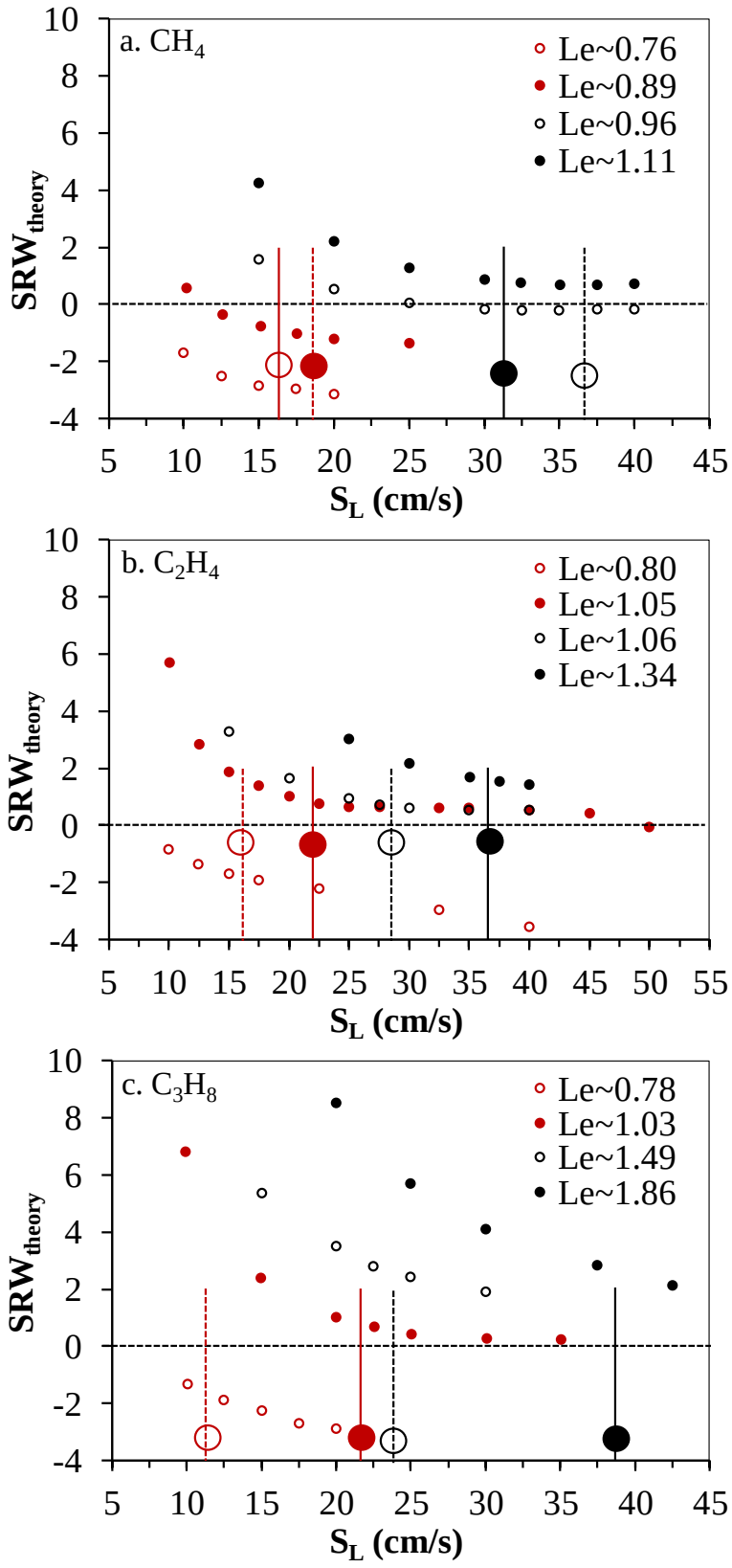

Fig. 10. Width of stability region in terms of acoustic velocity for a) CH_4 b) C_2H_4 c) C_3H_8 cases.

Experimental values of critical S_L for all cases are shown as vertical lines.

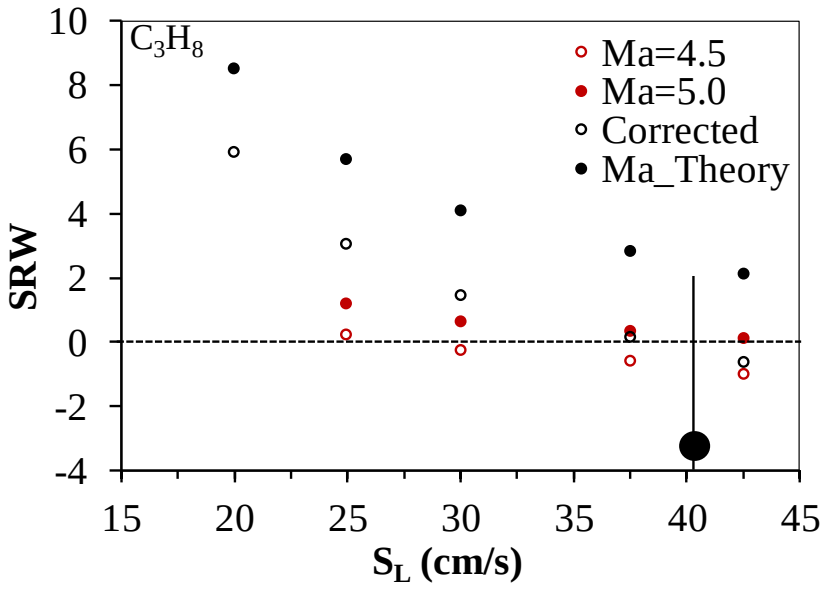

Fig. 11. *SRW* calculated using *Ma* of 4.5 and 5.0 compared with *Ma* obtained from Eqn. 7 for lean $C_3H_8/O_2/N_2$ mixtures. Corrected *SRW* obtained after applying the correction factor is also shown.

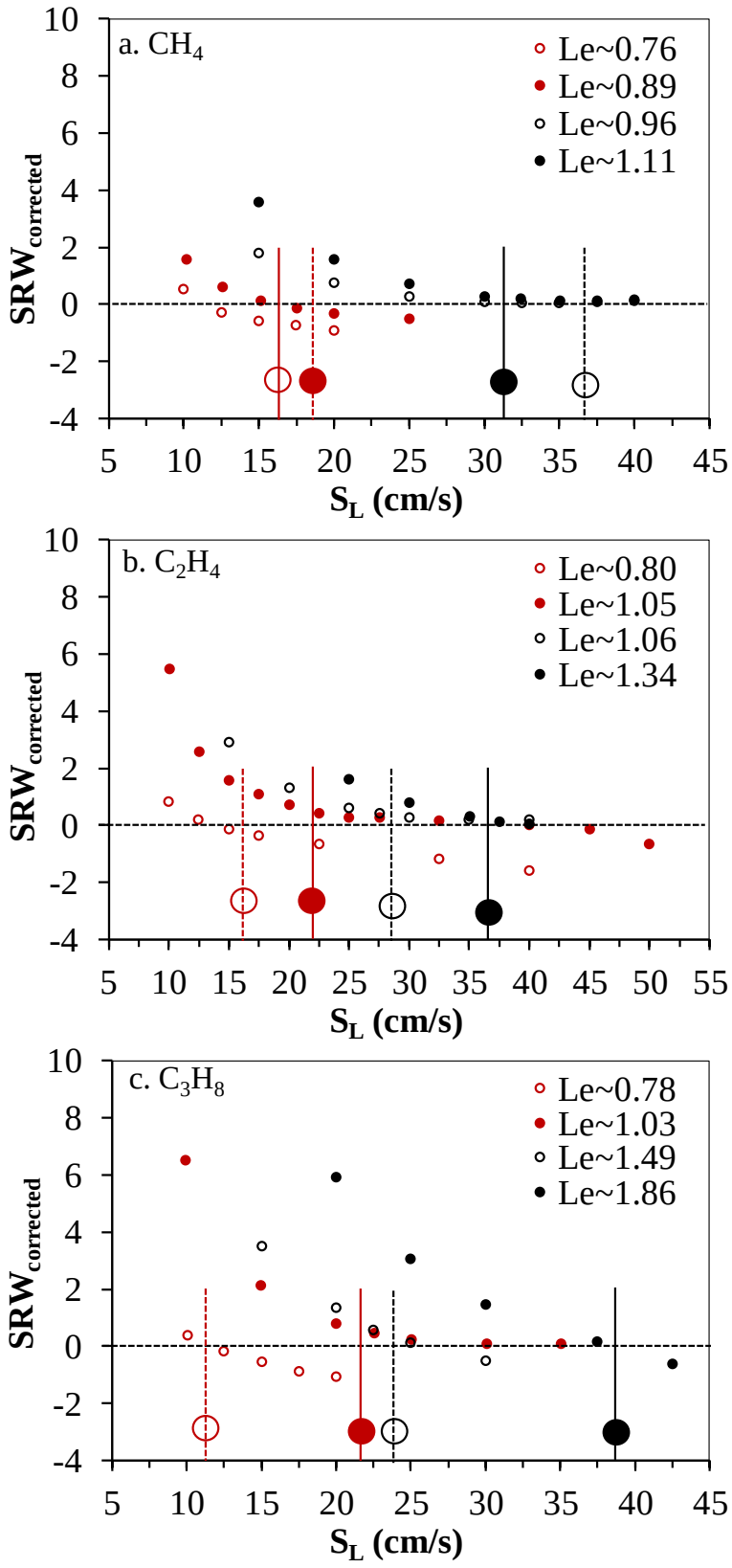

Fig. 12. *SRW* after employing correction for a) CH_4 b) C_2H_4 c) C_3H_8 cases. Experimental values of critical S_L for all cases are shown as vertical lines.